HHS Public Access

Author manuscript

Nanoscale. Author manuscript; available in PMC 2023 May 01.

Published in final edited form as:

Nanoscale. 2016 August 21; 8(31): 14877–14887. doi:10.1039/c6nr01637e.

Investigation of mechanism of bone regeneration in a porous biodegradable calcium phosphate (CaP) scaffold by a combination of a multi-scale agent-based model and experimental optimization/validation

Le Zhang[a,b,c,d], **Minna Qiao**[a], **Hongjie Gao**[a], **Bin Hu**[e], **Hua Tan**[f], **Xiaobo Zhou**[f], **Chang Ming Li**[b,c]

[a]College of Computer and Information Science, Southwest University, Chongqing 400715, P. R. China

[b]Institute for Clean Energy & Advanced Materials, Southwest University, Chongqing 400715, P.R. China

[c]Chongqing Key Laboratory for Advanced Materials and Technologies of Clean Energies, Chongqing 400715, P.R. China

[d]College of Mathematics and Statistics, Southwest University, Chongqing 400715, P. R. China

[e]School of Information Science and Engineering, Lanzhou University, Lanzhou 730000, P.R. China

[f]Department of Radiology, Wake Forest University School of Medicine, Winston-Salem, NC 27157, USA

Abstract

Herein, we have developed a novel approach to investigate the mechanism of bone regeneration in a porous biodegradable calcium phosphate (CaP) scaffold by a combination of a multi-scale agent-based model, experimental optimization of key parameters and experimental data validation of the predictive power of the model. The advantages of this study are that the impact of mechanical stimulation on bone regeneration in a porous biodegradable CaP scaffold is considered, experimental design is used to investigate the optimal combination of growth factors loaded on the porous biodegradable CaP scaffold to promote bone regeneration and the training, testing and analysis of the model are carried out by using experimental data, a data-mining algorithm and related sensitivity analysis. The results reveal that mechanical stimulation has a great impact on bone regeneration in a porous biodegradable CaP scaffold and the optimal combination of growth factors that are encapsulated in nanospheres and loaded into porous biodegradable CaP scaffolds layer-by-layer can effectively promote bone regeneration. Furthermore, the model is robust and able to predict the development of bone regeneration under specified conditions.

Keywords

Bone regeneration; Parameter estimation; Agent-based model; Experimental design; Porous biodegradable calcium phosphate (CaP) scaffold

1. Introduction

Bone reconstruction is a complex physiological process that exhibits nonlinear characteristics under different material and boundary conditions[2, 3]. The interaction between the external environment and internal factors makes the dynamic balance between osteoclasts and osteoblasts affect the formation of bone[4]. Recently, bone reconstruction has grown in significance in clinical studies due to its importance in human health. Nonetheless, because the microenvironment of bone growth is very complicated and involves various biological and physical processes, it is costly to perform *in vivo*/*in vitro* bone reconstruction experiments to investigate the bone formation process in detail. For this reason, this study proposes an *in silico* mathematics model that can not only simulate the bone reformation process within a porous biodegradable CaP scaffold under mechanical stimulation with a related experimental design, but can also predict the change in bone mass with respect to various growth factors that are encapsulated in nanospheres and loaded into porous biodegradable CaP scaffolds layer-by-layer after we optimize the key parameters and validate the predictive power of the model by experimental training and testing data.

Since the beginning of the 21st century, many biomaterials scientists have carried out many studies of bone reconstruction in different research areas such as the investigation of the relationship between osteoclasts and osteoblasts[4], osteogenic differentiation[5], mechanical stimulation of bone [6], cell mechanics[2], signalling pathways of bone cells [7, 8] and bone growth factors[9]. For example, Sun et al.[1] developed a multi-scale mathematical model, which not only reconstructed the 3D bone regeneration system and examined the effects of pore size and porosity on bone formation, but also studied the impact of growth factors on the change in bone mass. However, it did not take mechanical stimulation into consideration or use experimental design to investigate the priority of impact of bone mass-related growth factors. In addition, Checa et al.[10] developed a lattice-based mechanical platform to model tissue differentiation under conditions of angiogenesis, but it neither investigated the impact of the key growth factors on bone formation nor verified the predictive power of the model via experimental data. Recently, Sanz-Herrera et al.[11] constructed a mathematical model of bone tissue regeneration that can investigate a set of physiological processes associated with bone cells, such as porosity, mechanical properties and permeability, but it did not perform parameter analysis or validate the robustness of the model.

For the first time, this study has integrated mechanical stimulation, a data-mining algorithm and experimental design into our established 3D multi-scale model of bone reconstruction [1, 12]. Therefore, it can not only predict changes in bone mass under stimulation by different growth factors via experimental design, but also investigate the impact of mechanical stimulation on bone reformation. In particular, this study employed the currently widely used calcium phosphate (CaP) scaffolds, which are ideal materials for bone repair owing to their biocompatibility, adjustable degradation rates, and excellent bioactivity. The results demonstrate that not only can mechanical stimulation significantly promote the growth of active osteoblasts (OBa), pre-osteoblasts (OBp) and mesenchymal stem cells (MSC), but the model also has good predictive precision and robustness for the prediction

of bone regeneration and reveals the priority of the impact of growth factors on bone regeneration via experimental design.

2. Methods

This study developed a 3D multi-scale agent-based model of bone regeneration with four biological and physical scales, namely, molecular, cellular, scaffold, and bone tissue scales (Fig. 1). It not only employed a set of reaction-diffusion equations to describe the diffusion of growth factors released from the porous biodegradable CaP scaffold and the transportation of nutrients by the vasculature, but also used an agent-based module[13] to simulate the activities of bone cells under mechanical stimulation and the related signaling transduction pathway. Here, the biodegradable CaP scaffolds contained both human cells (MSC, osteocytes and endothelial cells) and growth factors for bone tissue repair.

Fig. 1 shows that stimulated by the growth factors diffused in the scaffold scale and regulated by the nutrient transported in the bone tissue scale, the signaling pathway in the molecular scale determines cell's phenotype switching on the cellular scale. On the contrary, cell's phenotype switch can remodel and impact the scaffold environment and the diffusion of the growth factors on the scaffold and bone tissue scale, respectively.

2.1 Molecular scale: the signaling pathway

Runx2 and Osterix (Osx) are two crucial transcription factors in osteoblast differentiation and bone regeneration (refer to Fig. 1 in Sun et al.[12]). As reported by previous studies[4], their expression can be regulated by the release of growth factors (BMP2 and Wnt) via the activation of intracellular proteins or related transcription factors such as Smad1/5 (S1), Smad2/3 (S2) and β-catenin[14].

The molecular regulatory mechanisms involved in the intracellular signalling pathway were modelled using a system of ordinary differential equations such as Eq. 1, as detailed in our previous research[12]. Values of the key parameters of Eq. 1 are listed in [1].

$$\frac{d[S1]}{dt} = \frac{V_1 \cdot [BMP2]}{K_1 \cdot [BMP2]} \cdot ([TotalS1] - [S1]) - d_1 \cdot [S1] \tag{1.1}$$

The change in concentration of phosphorylated Smad1/5 ($[S1]$) depends on the concentrations of BMP2 ($[BMP2]$) and unphosphorylated Smad1/5 ($[TotalS1] - [S1]$) and its dephosphorylation.

$$\frac{d[\beta Catenin]}{dt} = a - \left(\left(\frac{[Wnt] + b}{c \cdot [Wnt] + d}\right) \cdot \left(\frac{e}{e + [\beta Catenin]} + f\right) \cdot [\beta Catenin]\right) \tag{1.2}$$

where the concentrations of Wnt and β-catenin are represented by $[Wnt]$and $[\beta Catenin]$, respectively.

$$\frac{d[Runx2]}{dt} = \frac{V_1 \cdot [S1]}{K_1 + [S1]} + \frac{V_5 \cdot [S2]}{K_5 + [S2]} + \frac{V_6 \cdot [\beta Catenin]}{K_6 + [\beta Catenin]} - d_1 \cdot [Runx2] \quad (1.3)$$

Runx2[15] has been found to be a crucial transcription factor in osteogenic differentiation. Its expression and activation can be promoted by BMP2 via Smad1/5 and Smad2/3 ([$S2$]) and by Wnt ligands via β-catenin and other proteins. The concentration of Runx2 is represented by [$Runx2$].

$$\frac{d[Osx]}{dt} = \frac{V_7 \cdot [S1]}{K_7 + [S1]} + \frac{V_8 \cdot [Runx2]}{K_8 + [Runx2]} - d_5 \cdot [Osx] \quad (1.4)$$

Osx[16] is also a critical transcription factor in osteoblast differentiation, acting downstream of Runx2 and Smad1/5.

Here, the intracellular signaling pathway described by Eq. 1 is stimulated by the concentrations of the growth factors (BMP2, Wnt, Runx2 and Osx) released on the scaffold scale to determine the phenotype switch of the cell on the cellular scale.

2.2 Cellular scale: cell activities

2.2.1 Migration—MSC and OBp migrate along the gradient of the normalized concentration of growth factors, including bone morphogenetic protein 2 (BMP2), Wnt, and nutrients. The probability (P_i^{mig}) that MSC and OBp will migrate along the ith direction is given by Eq. 2. OBa is assumed not to migrate in this study, with reference to a previous report[17].

$$P_j^{mig} \propto (\nabla G_i + \nabla O_2) \cdot l_j, i = 1, 2, 3; j = 1, 2, \ldots, 6 \quad (2)$$

where G_i and O_2 are the concentrations of growth factors (BMP2 and Wnt ligands) and oxygen, respectively, and l_j is the directional vector along the jth direction. There are six directions in which a cell can migrate in our three-dimensional lattice.

2.2.2 Differentiation—Activated Runx2 and Osx play different roles in different stages of an osteoblastic lineage. Both Runx2 and Osx can promote the differentiation of MSC into OBp, whereas Runx2 can inhibit the differentiation of OBp into OBa[14, 18]. The probabilities that MSC will differentiate into OBp ($P_{MSC \to OBp}^{diff}$) and OBp will differentiate into OBa ($P_{OBp \to OBa}^{diff}$) are related to the levels of expression of activated Runx2 and Osx. We employ Hill functions[4] to model these situations by Eq. 3 and 4, as in previous studies[11].

$$P_{MSC \to OBp}^{diff} = \left(\frac{V_{D1, Runx2} \cdot [Runx2]}{K_{D1, Runx2} + [Runx2]} + \frac{V_{D1, Osx \cdot [Osx]}}{K_{D1, Osx} + [Osx]}\right) \cdot P_{MSC \to OBp}^{diff} \quad (3)$$

$$P_{OBp \to OBa}^{diff} = \left(\frac{1}{1 + [Runx2]/K_{D2, Runx2}} + \frac{V_{D2, Osx} \cdot [Osx]}{K_{D2, Osx} + [Osx]}\right) \cdot p_{OBp \to OBa}^{diff} \quad (4)$$

where $P^{diff}_{MSC\rightarrow OBp}$ and $P^{diff}_{OBp\rightarrow OBa}$ are the baseline probabilities that MSC will differentiate into OBp and OBp into OBa, respectively. Because both the concentration of oxygen and the strain[19] play major roles in the differentiation of MSC, we model this situation by the following rules (Fig. 2).

1. If (0.1 < S < 0.53) and O_2 is greater than Thr^{O^2}, then mature MSC differentiate towards OBa.
2. If (0.53 < S < 1) and O_2 is greater than Thr^{O^2}, then mature MSC differentiation towards OBp.
3. Otherwise, the direction of differentiation of MSC depends on Eq. 3 and 4, where Thr^{O^2} is the threshold of oxygen (O_2) concentration.

2.2.3 Proliferation—MSC, OBp and OBa can proliferate with different probabilities (p^{pro}). With reference to our previous research[20], we set these as constants. Here, Table 1 lists the values of the important parameters for the model.

2.2.4 Apoptosis—Because hyperbaric oxygen will attenuate cell apoptosis[26], Eq. 5 has been developed to describe the relation between the apoptosis rate of cells and the oxygen concentration. It is noted that if the oxygen concentration is less than the threshold (Th_{oxygen}), osteoblast cells will die.

$$P^{apop} = p_b^{apop} + \phi(O_2^{average} - O_2) \tag{5}$$

where p_b^{apop} and P^{apop} represent the baseline probability and probability of apoptosis of MSC, OBp and OBa, respectively, $O_2^{average}$ represents the normal oxygen concentration, an φ is a positive constant[11].

2.3 Scaffold scale: scaffold degradation and growth factor release

In the same way as in our previous research[12], growth factors are encapsulated in nanospheres and loaded into porous biodegradable CaP scaffolds layer-by-layer. After being implanted into defected bone, calcium phosphate can be degraded via hydration reactions and network breakage. The diffusion of the extracellular liquid and disintegration of calcium phosphate are described by Eq. 6 and 7, respectively:

$$\frac{\partial C}{\partial t} = D_C \nabla^2 C - k_C C M \tag{6}$$

$$\frac{\partial M}{\partial t} = -k_M C M \tag{7}$$

where C and M are the water concentration and molecular weight of calcium phosphate, respectively, D_C is the diffusivity of water, and k_C and k_M are the degradation rates for water and calcium phosphate, respectively.

BMP2, Wnt ligands and VEGF are released from the degrading CaP scaffold and continuously diffuse within the scaffold pores. The paracrine and autocrine activity of these cytokines are ignored because we assume that the concentrations of these cytokines secreted by individual cells are quite low compared with those released from the CaP scaffold. These processes are modeled by Eq. 8 [1]:

$$\frac{\partial G_i}{\partial t} = D_{G_i}\nabla^2 G_i + \chi_{scaffold} r_{G_i}(G_{i,\max} - G_i)\frac{C}{C + K_c} - \chi_{osteo} u_{G_i} G_i - d_{G_i} G_i \quad (8)$$

where D_{Gi} is the diffusivity of each growth factor, $G_{i,\max}$ is the maximum concentration of each growth factor initially loaded into the scaffold, r_{Gi} is the release constant, u_{Gi} is the depletion rate of the cytokine, d_{Gi} is the degradation rate and K_c is the Michaelis constant. The time-dependent characteristic function $\chi_{scaffold}(t, x)$ is equal to 1 in the calcium phosphate matrix and 0 in the pores of the scaffold. The value of $\chi_{osteo}(t, x)$ is equal to 1 if an osteoblastic cell is present at x; otherwise, it is equal to 0. Both $\chi_{scaffold}$ and χ_{osteo} are updated at each simulation step.

2.4 Bone tissue scale: angiogenesis and oxygen transportation

2.4.1 Angiogenesis—We assume that the motion of an individual endothelial cell located at the tip of a capillary sprout governs the motion of the entire sprout, and chemotaxis in response to VEGF gradients guides the motion of the endothelial cells at the tip of the capillary sprout. Eq. 9 defines the probability of migration of endothelial cells:

$$P_j \propto \alpha\frac{k_V}{k_V + v}\nabla V \cdot l_j, j = 1, 2, \cdots, 6 \quad (9)$$

where V is the concentration of VEGF, α is the chemotactic coefficient and K_V is a positive constant[27].

2.4.2 Nutrient transportation—Oxygen can be transported by the neovasculature to osteoblasts within scaffold pores, which is described by Eq. 10.

$$\frac{\partial O_2}{\partial t} = D_{O_2}\nabla^2 O_2 + \chi_{ves}(t, x) q_{O_2}(O_2^{blood} - O_2) - \chi_{osteo}(t, x) u_{O_2} O_2 \quad (10)$$

where D_{O_2} is the diffusivity of oxygen, q_{O_2} is the permeability of the vessel for oxygen, O_2^{blood} is the blood oxygen concentration, and u_{O_2} is the oxygen uptake rate of the cell.

2.5 Establish computational models by Abaqus[4]

Because our research aims to investigate the mechanism of bone regeneration in a porous biodegradable calcium phosphate (CaP) scaffold[1], we have to consider the impacts of nutrient transportation, growth factors, angiogenesis, and mechanical stimulation together from the biological perspective of the system. In particular, because biodegradable material is used to repair the bone tissue scaffold, it indirectly affects mechanical stimulation via regulating the release of cytokines owing to its material properties. However, because mechanical stimulation is sufficiently complicated, this study integrates a well-established

mechanical stimulation[11] module into the model to study the mechanism of bone regeneration as follows.

The time course of tissue formation and vascularization of the scaffold is modeled as an iterative process (Fig. 2a). Fig. 2b shows how to compute the number of cells in each sub-cube at each run. The densities of mature bone consisting of OBp ($Density_p$) and immature bone consisting of OBa ($Density_a$) are described by Eq. 11.1 and Eq. 11.2, respectively:

$$Density_p = N_{OBp}/V_{sc} \tag{11.1}$$

$$Density_a = N_{OBa}/V_{sc} \tag{11.2}$$

where N_{OBp} and N_{OBa} represent the number of OBp and OBa, respectively, and V_{sc} is the volume of the sub-cube.

The computation of stress for each small cube (Fig. 2b) is illustrated as follows.

1. For each sub-cube, if $Density_p$ is greater than $Density_a$, then the material type of the sub-cube is set to immature bone; otherwise, it is set to mature bone.
2. Eq. 12.1 and Eq. 12.2 are employed to compute the Young's modulus[4] of immature and mature bone, respectively:

$$E = Density \times S_p \tag{12.1}$$

$$E = Density \times S_a \tag{12.2}$$

where S_p and S_a represent the speed of propagation of sound in immature and mature bone, respectively.

3. The stress (S) for each sub-cube can be computed by Eq. 13.

$$S = E \times D \tag{13}$$

where D is the strain of the sub-cube[4].

2.6 Model training and testing

To make the results of the model believable, this study optimized the key parameters and estimated the predictive capacity of the model by using experimental data (Table 2) and a data-mining algorithm. The experimental data were obtained on the designated days after treating MSCs with BMP2 on day 1 followed by Wnt on day 4. Alkaline phosphatase (ALP) and double-stranded DNA (dsDNA) are two critical biomarkers for quantifying the early differentiation rate of MSC towards OBp and the total cell number, respectively.

A particle swarm optimization (PSO) algorithm[28] was used to train two key parameters (Thr^{O^2} and V_i) of the model by fitting the simulated data against the experimental data using

Eq. 14. Thr^{O^2} and V_i represent the oxygen concentration and the speed of propagation of sound in the material, respectively:

$$\Theta^* = \operatorname{argmin} \sum_{i=1}^{N} \sum_{j=1}^{T} \omega (x_i^{sim}(t_j, \Theta) - x_i^{\exp}(t_j))^2 \tag{14}$$

where $\omega_i = 1 \Big/ (\max_j x_i^{\exp}(t_j))^2$, N and T denote the number of cells and time points, respectively, and $x_i^{sim}(t_j, \Theta)$ and $x_i^{\exp}(t_j)$ represent the number of cells at each time step of the simulation and experiment, respectively.

Eq. 15 was used to compute the average relative error (ARE)[17, 29, 30] for testing the predictive precision of the model:

$$ARE = \sum_{i=1}^{R} \frac{| Est\theta_i - L\theta |}{R \times | L\theta |} \times 100\,\% \tag{15}$$

where R represents the number of repetitions for the simulation and $Est\theta_i$ and $L\theta$ represent the simulated and experimental results, respectively.

3. Results

This section consists of the following three major results. Firstly, we investigate the effects of mechanical stimulation, angiogenesis and bone formation in detail after the 3D bone regeneration system within a porous biodegradable CaP scaffold is developed. Secondly, we compare the changes in bone mass between the presence and absence of mechanical stimulation. Thirdly, we employ training data to optimize the key parameters of the model and use testing data to validate the predictive power of the model, as well as analyzing the robustness of the model by sensitivity analysis.

3.1 Simulation of 3D vascularized bone regeneration

Based on our previous research[1], we reconstruct the system of vascularized bone regeneration within the 3D porous CaP scaffold, which consists of the coupled processes of the evolution of scaffold degradation (Eq. 6 and 7), exogenous growth factor release (Eq. 8), angiogenesis (Eq. 9), differentiation of MSCs (Eq. 3 and 4), and cell growth within the scaffold pores over time.

This research incorporates mechanical stimulation into the well-developed model of 3D bone regeneration[1] within a porous biodegradable CaP scaffold to investigate the impact of mechanical stimulation on bone regeneration. More importantly, because the dynamics of the differentiation of MSCs will cause changes in OBs as described by Eq. 3, it is directly related to the bone mass. Fig. 3 shows a 2/3D simulation of the bone regeneration process under mechanical stimulation. On day 10, blood vessels were rare and scattered on the surface of the porous CaP scaffold (Fig. 3a and d); on day 20, newly formed blood vessels grew into the pores located at the periphery of the scaffold and several blood vessels started branching to form a tree (Fig. 3b and e). On day 28, a branched vasculature was observed

within the peripheral pores of the scaffold and a few blood vessels were already growing into the pores at the center of the scaffold (Fig. 3c and f).

Fig. 4 shows the dynamics of the various cells over time in the presence and absence of mechanical stimulation within a porous biodegradable CaP scaffold. The changes in the trend in the cell numbers for MSC, OBa and OBp are similar regardless of the presence or absence of mechanical stimulation, but Fig. 4a, b and c indicate that mechanical stimulation will significantly increase the cell numbers for these three types of cell after 28 days, especially for OBa. The numbers of MSC, OBa and OBp increased in the beginning and decreased after reaching peaks at different times. The number of MSC peaked around day 3 (Fig. 4a), that of OBa peaked around day 7 (Fig. 4b), and that of OBp peaked around day 14 (Fig. 4c).

3.2 Training and testing of the model

The predictive power of the model was verified by fitting the simulated results against the experimental results. A PSO algorithm [31] was employed to train the model by setting the initial values of the key parameters and the training data. The refinement step was repeated five times to obtain optimal and stable results (Fig. 5), which show a similarity between the simulated and experimental results after the model training process. We define the important variables and equations for the testing and training of the model in Table 3.1, and list the related results in Table 3.2.

In the training process, simulated data ($CS_1^{MSC\rightarrow OBp}$ and $CS_2^{MSC\rightarrow OBp}$) were employed to optimize the key parameters of the model by fitting them against experimental data ($CE_1^{MSC\rightarrow OBp}$ and $CE_2^{MSC\rightarrow OBp}$). In the testing process, a leave-one-out cross-validation (LOOCV) [32] algorithm was employed to validate the predictive power of the model by using three time points of the experimental data as the training data set ($CS_2^{MSC\rightarrow OBp}$ and $CS_3^{MSC\rightarrow OBp}$) for the key parameters of the optimization of the model and the remaining time points of the experimental data as the testing data set ($CE_2^{MSC\rightarrow OBp}$ and $CE_3^{MSC\rightarrow OBp}$) for computation of the accuracy of the model (Eq. 16). The small relative error (RE) indicates high predictive accuracy.

$$RE = \frac{\chi_i^{\sin}(t_j, \theta) - \chi_i^{\exp}(t_j)}{\chi_i^{\exp}(t_j)} \tag{16}$$

As computed by Eq. 16, the average and standard deviation of the predictive power of the model are 62.21% and 0.019, respectively.

3.3 Parameter sensitivity analysis in our model

Sensitivity analysis [17] was employed to evaluate the impact of the parameters on the behavior of the model. The value of each parameter in Table 4.1 was varied independently over the specified range [17] about 10 times, while keeping the values of the other parameters the same as their baseline. Table 4.2 lists the Spearman rank-order correlation coefficient [33] and p value for each parameter. Also, Table 4.2 shows that the parameters

V_6, K_6, d_1, S_p, and S_a are sensitive to OBp, the parameters V_6, d_1, V_8, d_s, S_p, and S_a are sensitive to OBa, and the parameters S_p and S_a are sensitive to MSC.

3.4 Significance of effects of growth factors on bone formation

It is well known that using orthogonal experimental design [34] can reduce the number of experiments. Therefore, an orthogonal test table L9(34) [35, 36] was employed to investigate which single growth factor or combination of these growth factors (VEGF, BMP2 and Wnt) will most effectively promote bone formation. Therefore, three major growth factors (BMP2, VEGF and Wnt) were set as the experimental factors (columns 2, 3 and 4 in Table 5.1) for the experimental design with three levels: high (10), medium (5) and low (0), in accordance with the principles of experimental design [35, 36]. The cumulative number of OBa was set as the experimental test index [37] to represent the bone mass at the designated times (columns 5 and 6 in Table 5.1) in the experimental design, because the growth rate of bone mass is proportional to the number of OBa. Table 5.1 shows that the number of OBa under mechanical stimulation is greater than the number of OBa not under mechanical stimulation. Table 5.2 and Table 5.3 [35, 37] indicate that the optimal combination of experimental factors is always BMP2 (medium), VEGF (medium) and Wnt (high), and the order of priority of the growth factors (BMP2 > VEGF > Wnt) is statistically significant regardless of mechanical stimulation, respectively.

4. Discussion

This study considers the impact of angiogenesis on bone growth [26]. Fig. 3a, b and c demonstrate that angiogenesis can promote the accumulation of VEGF in the center of the porous biodegradable CaP scaffold rather than on the surface, whereas new blood vessels will start growing on the surface of the porous biodegradable CaP scaffold rather than in the center because of inhibition by the wall of the porous biodegradable CaP scaffold. These phenomena imply that blood vessels will develop much faster in the loose structure of the scaffold rather than in the dense structure, and also that a more uniform distribution of VEGF in the scaffold will significantly promote the growth of blood vessels. Moreover, Fig. 3d shows that the initial porous biodegradable CaP scaffold has a pore structure, whereas Fig. 3e and f show that the porous biodegradable CaP scaffold moves into the center of the bone over time. This phenomenon demonstrates that the scaffold made from calcium phosphate is hydrolyzed during bone regeneration, as was expected.

As reported by previous research [1], because mechanical stimulation will result in the differentiation of more MSC to OBa and OBp, it will increase the bone mass density and finally change the material properties. Here, Fig. 4 indicates that mechanical stimulation plays a role in bone regeneration, because the numbers of the three kinds of cells (MSC, OBp and OBa) under mechanical stimulation are significantly greater than the number not under mechanical stimulation, while they display almost the same dynamic trend. Also, Fig. 4 indicates that the decreasing trend in the numbers of MSC, OBp and OBa slows down around day 10, because mechanical stimulation significantly changes the rate of differentiation of MSC to OBa or OBp (Fig. 2a).

After the training (Fig. 4), testing (Fig. 5) and sensitivity analysis (Table 4.2) procedures, the model is robust enough to predict bone regeneration with high accuracy.

The small p values in Table 4.2 indicate that the parameters (V_6 and d_1) that determine the expression of Runx2 are significantly related to OBp and OBa, and also that the parameters (V_8 and d_s) that determine the expression of Osx are significantly related to OBa. These results prove that Runx2 actually plays an important role in promoting the differentiation of MSCs into OBp and inhibiting the differentiation of OBp into OBa [38], and also that Osx will promote OBa via the intracellular signaling pathway [4].

Finally, experimental design was employed to investigate the impact of key growth factors such as BMP2 and Wnt on bone regeneration. By comparing the number of OBa (Table 5.1 and 5.2) in the presence and absence of mechanical stimulation, we can conclude that mechanical stimulation is positively related to bone regeneration. Also, Table 5.3 demonstrates that the priority of the impact of the key growth factors is regardless of mechanical stimulation.

In brief, this model can not only predict vascular bone regeneration by using experimental data [39] and a data-mining algorithm [40], but can also employ experimental design [41] to investigate which growth factors play major roles in bone regeneration under mechanical stimulation within the porous biodegradable calcium phosphate (CaP) scaffold. However, it does not consider the impact of sequential drug delivery or employ the experimental data to optimize the key parameters of the related signaling transduction pathway. Therefore, we are going to develop related biological experiments and mathematical models to investigate potential cytokine combinations, optimal drug doses and drug delivery sequences within the porous biodegradable CaP scaffold in the near future.

Acknowledgments

This work is supported by the National Science Foundation of China under Grant No. 61372138, Chongqing excellent youth award, the Chinese Recruitment Program of Global Youth Experts, Chongqing Key Laboratory for Advanced Materials and Technologies of Clean Energies, Fundamental Research Funds for the Central Universities of China No. XDJK2014B012 and No. XDJK2016A003, as well as USA NIH grant U01CA166886-01.

Notes and references

1. Sun X, Kang Y, Bao J, Zhang Y, Yang Y, Zhou X. Modeling vascularized bone regeneration within a porous biodegradable CaP scaffold loaded with growth factors. Biomaterials. 34: 4971–4981. 2013. [PubMed: 23566802]
2. Ahmed EG. Bone reconstruction: from bioceramics to tissue engineering. Expert Review of Medical Devices. 2: 87–101. 2005. [PubMed: 16293032]
3. Burg KJL, Porter S, Kellam JF. Biomaterial developments for bone tissue engineering. Regulatory Peptides. 21: 2347–2359. 2000.
4. Vincent L, Tobin FL, Greller LD, Cho CR, Suva LJ. Modeling the interactions between osteoblast and osteoclast activities in bone remodeling. Journal of Theoretical Biology. 229: 293–309. 2004. [PubMed: 15234198]
5. Neelam J, Haynesworth SE, Caplan AI, Bruder SP. Osteogenic differentiation of purified, culture - expanded human mesenchymal stem cells in vitro. Journal of Cellular Biochemistry. 64: 295–312. 1997. [PubMed: 9027589]

6. Checa S, Prendergast PJ. Effect of cell seeding and mechanical loading on vascularization and tissue formation inside a scaffold: a mechano-biological model using a lattice approach to simulate cell activity. J Biomech. 43: 961–8. Mar 22. 2010; [PubMed: 19954779]
7. Miller, FP, Vandome, AF, Mcbrewster, J. Cell signaling. Alphascript Publishing; 2010.
8. Kholodenko BN. Cell-signaling dynamics in time and space. Nature Reviews Molecular Cell Biology. 7: 2006;
9. Schilephake H. Bone growth factors in maxillofacial skeletal reconstruction. International Journal of Oral & Maxillofacial Surgery. 31: 469–84. 2002. [PubMed: 12418561]
10. Sandino C, Checa S, Prendergast PJ, Lacroix D. Simulation of angiogenesis and cell differentiation in a CaP scaffold subjected to compressive strains using a lattice modeling approach. Biomaterials. 31: 2446–52. Mar. 2010; [PubMed: 19969348]
11. Sanz-Herrera JA, Garcia-Aznar JM, Doblare M. A mathematical model for bone tissue regeneration inside a specific type of scaffold. Biomechanics & Modeling in Mechanobiology. 7: 355–66. 2007. [PubMed: 17530310]
12. Xiaoqiang S, Jing S, Jiguang B, Tao P, Le Z, Yuanyuan Z, et al. Cytokine combination therapy prediction for bone remodeling in tissue engineering based on the intracellular signaling pathway. Biomaterials. 33: 8265–8276. 2012. [PubMed: 22910219]
13. Bonabeau E. Agent-Based Modeling: Methods and Techniques for Simulating Human Systems. Proceedings of the National Academy of Sciences. 99 (Suppl 3) 7280–7. 2002.
14. Gordeladze JO, Reseland JE, Isabelle DR, Florence A, Christian J. From stem cells to bone: phenotype acquisition, stabilization, and tissue engineering in animal models. Ilar Journal. 51: 42–61. 2009. [PubMed: 20075497]
15. Zelzer E, Glotzer DJ, Hartmann C, Thomas D, Fukai N, Soker S, et al. Tissue specific regulation of VEGF expression during bone development requires Cbfa1/Runx2. Mechanisms of Development. 106: 97–106. 2001. [PubMed: 11472838]
16. Celil AB, Hollinger JO, Campbell PG. Osx transcriptional regulation is mediated by additional pathways to BMP2/Smad signaling. Journal of Cellular Biochemistry. 95: 518–28. 2005. [PubMed: 15786511]
17. Qiao M, Wu D, Carey M, Zhou X, Zhang L. Multi-Scale Agent-Based Multiple Myeloma Cancer Modeling and the Related Study of the Balance between Osteoclasts and Osteoblasts. Plos One. 10: 2015.
18. Komori T. Regulation of bone development and maintenance by Runx2. Frontiers in Bioscience A Journal & Virtual Library. 13: 898–903. 2008. [PubMed: 17981598]
19. Huiskes R, Driel WDV, Prendergast PJ, Søballe K. A biomechanical regulatory model for periprosthetic fibrous-tissue differentiation. Journal of Materials Science Materials in Medicine. 8: 785–788. 1997. [PubMed: 15348791]
20. Sun X, Le Z, Hua T, Bao J, Strouthos C, Zhou X. Multi-scale agent-based brain cancer modeling and prediction of TKI treatment response: Incorporating EGFR signaling pathway and angiogenesis. Bmc Bioinformatics. 13: 1–14. 2012. [PubMed: 22214541]
21. Checa S, Prendergast PJ. A Mechanobiological Model for Tissue Differentiation that Includes Angiogenesis: A Lattice-Based Modeling Approach. Annals of Biomedical Engineering. 37: 129–45. 2008. [PubMed: 19011968]
22. Artel A, Mehdizadeh H, Chiu YC, Brey EM, Cinar A. An Agent-Based Model for the Investigation of Neovascularization Within Porous Scaffolds. Tissue Engineering Part A. 17: 2133–41. 2011. [PubMed: 21513462]
23. Sanzherrera JA, Garcíaaznar JM, Doblaré M. A mathematical approach to bone tissue engineering. Philosophical Transactions of the Royal Society A Mathematical Physical & Engineering Sciences. 367: 2055–78. 2009.
24. Kang HS. Hirarchical Design and Simulation of Tissue Engineering Scaffold Mechanical, Mass Transport, and Degradation Properties. 2010.
25. Davis HE, Leach JK. Designing Bioactive Delivery Systems for Tissue Regeneration. Annals of Biomedical Engineering. 39: 1–13. 2011. [PubMed: 20676773]

26. Clara S, Sara C, Prendergast PJ, Damien L. Simulation of angiogenesis and cell differentiation in a CaP scaffold subjected to compressive strains using a lattice modeling approach. Biomaterials. 31: 2446–52. 2009. [PubMed: 19969348]
27. Wang J, Le Z, Jing C, Gang Y, Wu H, Miao H, et al. Multi-scale agent-based modeling on melanoma and its related angiogenesis analysis. Theoretical Biology & Medical Modelling. 10: 41–41. 2013. [PubMed: 23800293]
28. Zhou C, Gao HB, Gao L, Zhang WG. Particle Swarm Optimization(PSO) Algorithm. Application Research of Computers. 2003.
29. Farnum NR. Improving the Relative Error of Estimation. American Statistician. 44: 288–289. 1990.
30. Tong X, Chen J, Miao H, Li T, Zhang L. Development of an Agent-Based Model (ABM) to Simulate the Immune System and Integration of a Regression Method to Estimate the Key ABM Parameters by Fitting the Experimental Data. Plos One. 10: 2015;
31. Zhang, W; Liu, Y; Clerc, M. An adaptive PSO algorithm for reactive power optimization. Advances in Power System Control, Operation and Management, 2003. ASDCOM 2003. Sixth International Conference on (Conf. Publ. No. 497); 2003. 302–307.
32. Cawley GC, Talbot NLC. Efficient leave-one-out cross-validation of kernel fisher discriminant classifiers. Pattern Recognition. 36: 2585–2592. 2003.
33. Zar JH. Significance Testing of the Spearman Rank Correlation Coefficient. Journal of the American Statistical Association. 67: 578–580. 1972.
34. Song Q. Effects of Apparatus Parameters on MFL Signals Using Orthogonal Experimental Design. Applied Mechanics & Materials. 44: 3524–3528. 2010.
35. Shieh G, Jan SL. Optimal sample size allocation for Welch's test in one-way heteroscedastic ANOVA. Behavior Research Methods. 47: 374–383. 2014.
36. Yanfeng QU, Wang X, Dianyu YU, Zhang Z, Qian L. Optimization of Technology for Rice Bran Oil Bleaching. Journal of Shihezi University. 2012.
37. Fan Y, Ma Y, Lu H, Deng R, College T, University N. An Optimization Design of the Ethanol Gasoline Engine Intake System Based on the Orthogonal Test. Agricultural Equipment & Vehicle Engineering. 2014.
38. Loebel C, Czekanska E, Bruderer M, Salzmann GM, Alini M, Stoddart MJ. In vitro osteogenic potential of human bone marrow derived MSCs is predicted by Runx2/Sox9 Ratio. Tissue Engineering Part A. 2014.
39. Lian JB, Stein GS. The developmental stages of osteoblast growth and differentiation exhibit selective responses of genes to growth factors (TGF beta 1) and hormones (vitamin D and glucocorticoids). Journal of Oral Implantology. 19: 95–105. 1993; [PubMed: 8246305]
40. Han J, Kamber M. Data Mining: Concepts and Technologies. Data Mining Concepts Models Methods & Algorithms Second Edition. 5: 1–18. 2001.
41. Mason, RL, Gunst, RF, Hess, JL. Statistical Principles in Experimental Design. John Wiley & Sons, Inc; 2003.

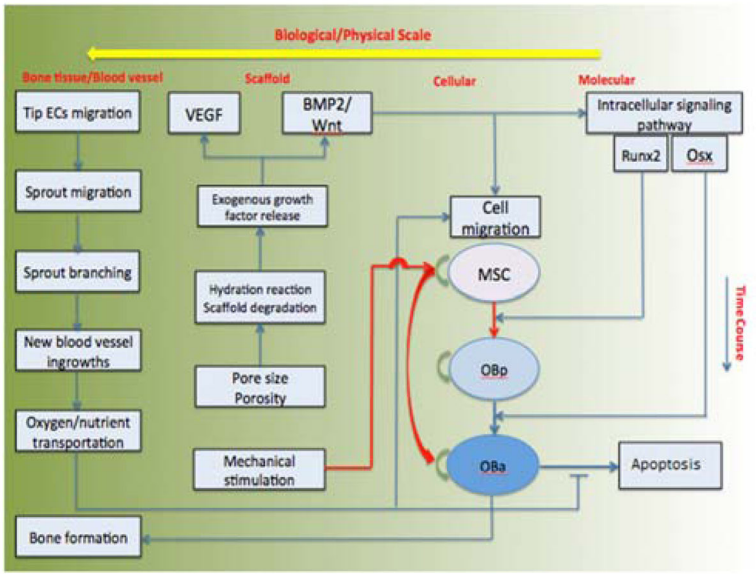

Figure 1.
Schematic of the computational flow

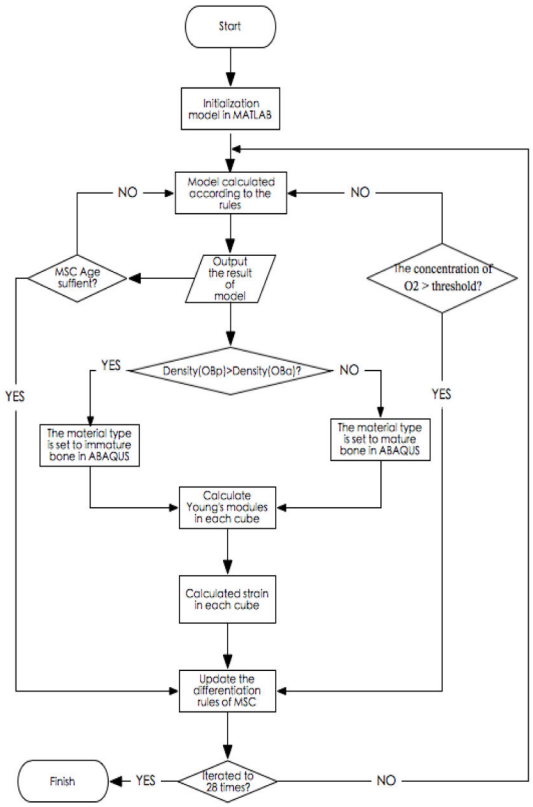

(a)

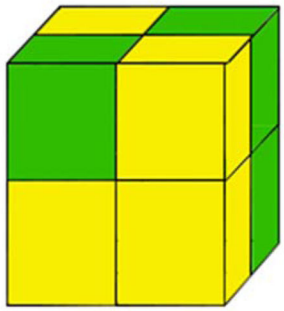

(b)

Figure 2.
(a) Workflow of the computational algorithm (b) Finite element analysis model

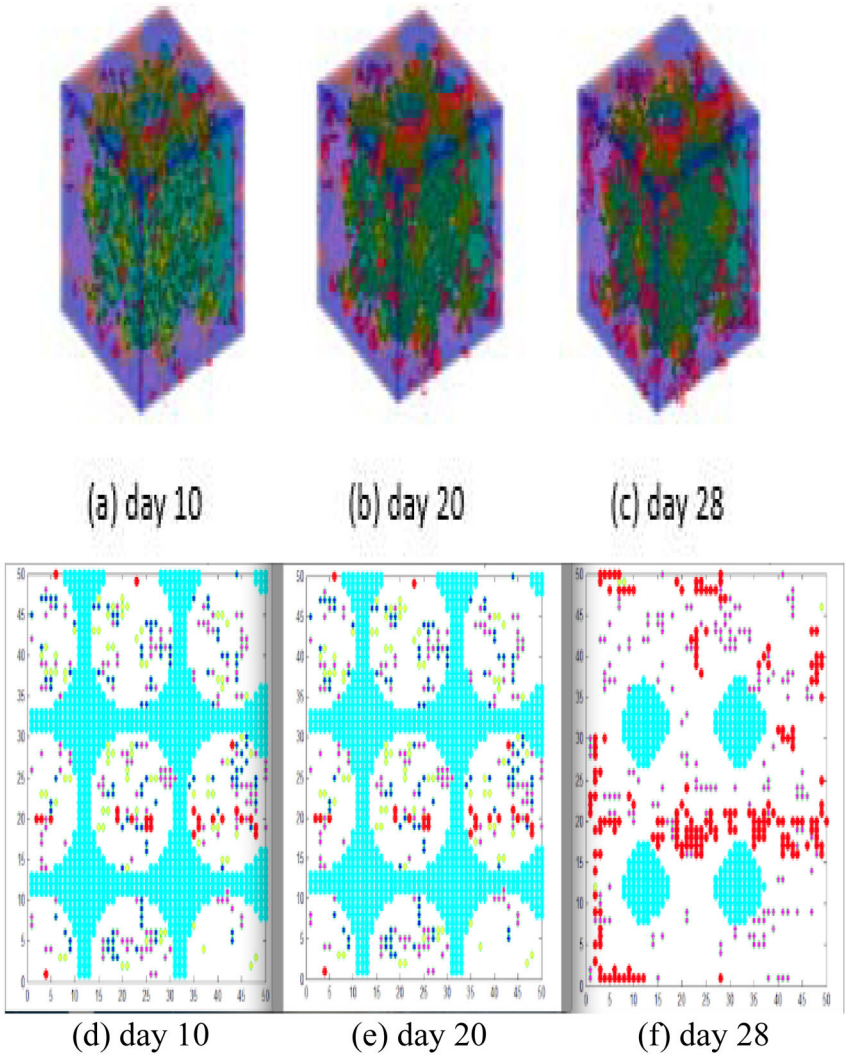

Figure 3.

3D bone formation and 2D slices of bone formation over time. (a), (b) and (c) show the 3D model under mechanical stimulation on days 10, 20 and 28, respectively. (d), (e) and (f) show 2D slices of bone formation on days 10, 20 and 28, respectively. The porous CaP scaffold, MSC, OBa, angiogenesis and pore structure are colored cyan, yellow, blue, red and white, respectively.

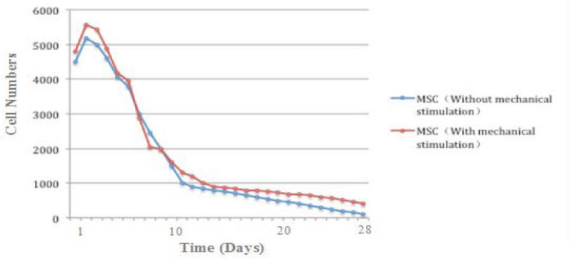

(a)

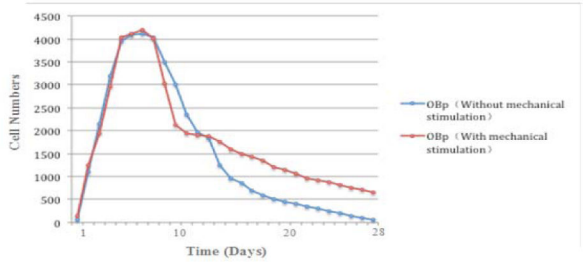

(b)

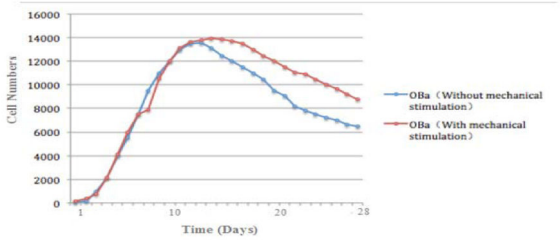

(c)

Figure 4.
Dynamics of MSC (a), OBp (b) and OBa (c) over 28 days.

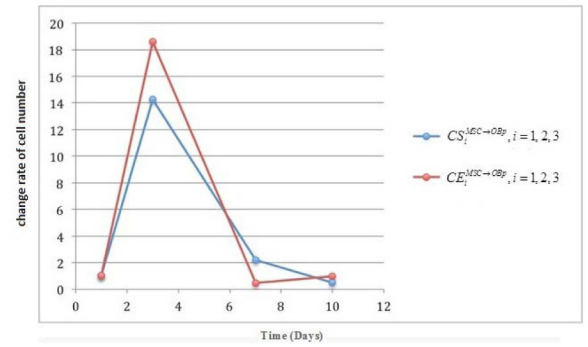

(a)

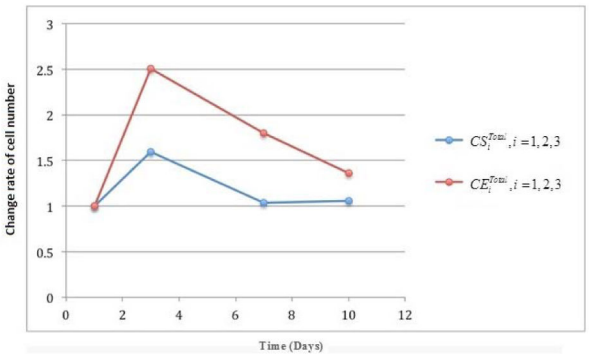

(b)

Figure 5.
Results of training (a) and testing (b)

Table 1

Values of the important parameters for the model

Symbol	Value	Unit	Description	Reference
$p_{MSC\rightarrow OBp}^{diff}$	0.3	Day^{-1}	Differentiation rate of MSC to OBp	[6, 10, 21]
$p_{OBp\rightarrow OBa}^{diff}$	0.3	Day^{-1}	Differentiation rate of OBp to OBa	[6, 10, 21]
$K_{D1,\ Runx\,2}$	500	[−]	Regulation coefficient 1 regarding Runx2	[12]
$K_{D1,\ Osx}$	4000	[−]	Regulation coefficient 1 regarding Osx	[12]
$V_{D1,\ Runx\,2}$	8000	[−]	Hill regulatory factor 1 regarding Runx2	[12]
$V_{D1,\ Osx}$	4×10^4	[−]	Hill regulatory factor 1 regarding Osx	[12]
$K_{D2,Runx2}$	0.8	[−]	Regulation coefficient 2 regarding Runx2	[12]
$K_{D2,\ Osx}$	100	[−]	Regulation coefficient 2 regarding Osx	[12]
p^{pro}	0.6	Day^{-1}	Proliferation rate of MSC and OBp	[6, 10, 21]
p_{MSC}^{apop}	0.05	Day^{-1}	Apoptosis rate of MSC	[6, 10, 21]
p_{OBp}^{apop}	0.10	Day^{-1}	Apoptosis rate of OBp	[6, 10, 21]
p_{OBa}^{apop}	0.16	Day^{-1}	Apoptosis rate of OBa	[6, 10, 21]
ϕ	125	[−]	Positive constant	Estimated
th_{oxygen}	0.0015	[−]	Threshold of cell apoptosis	Estimated
D_C	6.7×10^{-8}	$cm^2\ s^{-1}$	Diffusivity of water	[22]
k_C	0.15	[−]	Degradation rate of water	[23]
k_M	0.15	[−]	Degradation rate of CaP molecular weight	[23]
$D_{G\,i}$	1.55×10^{-5}	$cm^2\ s^{-1}$	Diffusivity of growth factor in water	[24]
$r_{G\,i}$	0.2	[−]	Growth factor release constant	Estimated
$u_{G\,i}$	10	$ng/10^6$ cells/day	Depletion rate of cytokine by osteoblastic cells	[25]
$d_{G\,i}$	0.03	Day^{-1}	Degradation rate of cytokine	[25]
K_C	0.5	[−]	Michaelis constant	Estimated
a	2600	$cm^2 s^{-1} M^{-1}$	Chemotactic coefficient	[20]
k_V	1.67×10^{-10}	[−]	Positive constant controlling chemotactic sensitivity	[20]
D_N	8×10^{-5}	$cm^2 s^{-1}$	Diffusivity of oxygen	[20]
q_N	0.5	[−]	Vessel permeability for oxygen	[20]
N^{blood}	0.0025	[−]	Blood oxygen concentration	[20]
u_N	6.25×10^{-4}	[−]	Cell uptake rate of oxygen	[20]

Table 2

ALP and dsDNA data

	ALP		dsDNA	
Day	**Mean**	**SD**	**Mean**	**SD**
1	8.643728	0.499756	0.138832	0.005635
3	160.7598	7.218334	0.348147	0.017524
7	74.13583	6.928568	0.361439	0.031959
10	73.31991	10.62254	0.491355	0.067455

Table 3

(1) Definitions of the parameters for model testing; (2) comparison between experimental and simulated results

(1)

Parameter definition	Description
$CS_1^{MSC\rightarrow OBp} = \frac{SN_3^{MSC\rightarrow OBp} - SN_1^{MSC\rightarrow OBp}}{SN_1^{MSC\rightarrow OBp}}$	$CS_1^{MSC\rightarrow OBp}$ is the rate of change in the differentiation of MSC to OBp during days 1 to 3 in the simulation.
$CS_2^{MSC\rightarrow OBp} = \frac{SN_7^{MSC\rightarrow OBp} - SN_3^{MSC\rightarrow OBp}}{SN_3^{MSC\rightarrow OBp}}$	$CS_2^{MSC\rightarrow OBp}$ is the rate of change in the differentiation of MSC to OBp during days 3 to 7 in the simulation.
$CS_3^{MSC\rightarrow OBp} = \frac{SN_{10}^{MSC\rightarrow OBp} - SN_7^{MSC\rightarrow OBp}}{SN_7^{MSC\rightarrow OBp}}$	$CS_3^{MSC\rightarrow OBp}$ is the rate of change in the differentiation of MSC to OBp during days 7 to 10 in the simulation.
$CE_1^{MSC\rightarrow OBp} = \frac{EN_3^{MSC\rightarrow OBp} - EN_1^{MSC\rightarrow OBp}}{EN_1^{MSC\rightarrow OBp}}$	$CE_1^{MSC\rightarrow OBp}$ is the rate of change in the differentiation of MSC to OBp during days 1 to 3 in the experiment.
$CE_2^{MSC\rightarrow OBp} = \frac{EN_7^{MSC\rightarrow OBp} - EN_3^{MSC\rightarrow OBp}}{EN_3^{MSC\rightarrow OBp}}$	$CE_2^{MSC\rightarrow OBp}$ is the rate of change in the differentiation of MSC to OBp during days 3 to 7 in the experiment.
$CE_3^{MSC\rightarrow OBp} = \frac{EN_{10}^{MSC\rightarrow OBp} - EN_7^{MSC\rightarrow OBp}}{EN_7^{MSC\rightarrow OBp}}$	$CE_3^{MSC\rightarrow OBp}$ is the rate of change in the differentiation of MSC to OBp during days 7 to 10 in the experiment.
$CS_1^{Total} = \frac{SN_3^{Total} - SN_1^{Total}}{SN_1^{Total}}$	CS_1^{Total} is the rate of change in the total cell number during days 1 to 3 in the simulation.
$CS_2^{Total} = \frac{SN_7^{Total} - SN_3^{Total}}{SN_3^{Total}}$	CS_2^{Total} is the rate of change in the total cell number during days 3 to 7 in the simulation.
$CS_3^{Total} = \frac{SN_{10}^{Total} - SN_7^{Total}}{SN_7^{Total}}$	CS_3^{Total} is the rate of change in the total cell number during days 7 to 10 in the simulation.

(1)

Parameter definition	Description
$CE_1^{Total} = \frac{EN_3^{Total} - EN_1^{Total}}{EN_1^{Total}}$	CE_1^{Total} is the rate of change in the total cell number during days 1 to 3 in the experiment.
$CE_2^{Total} = \frac{EN_7^{Total} - EN_3^{Total}}{EN_3^{Total}}$	CE_2^{Total} is the rate of change in the total cell number during days 3 to 7 in the experiment.
$CE_3^{Total} = \frac{EN_{10}^{Total} - EN_7^{Total}}{EN_7^{Total}}$	CE_3^{Total} is the rate of change in the total cell number during days 7 to 10 in the experiment.

(2)

	Differentiation of MSC to OBp				Total number of cells			
$CS_1^{MSC \to OBp}$	14.250	$CE_1^{MSC \to OBp}$	18.598433	CS_1^{Total}	1.595570	CE_1^{Total}	2.507686
$CS_2^{MSC \to OBp}$	2.202786	$CE_2^{MSC \to OBp}$	0.467379	CS_2^{Total}	1.797395	CE_2^{Total}	1.038179
$CS_3^{MSC \to OBp}$	0.498009	$CE_3^{MSC \to OBp}$	0.9758315	CS_3^{Total}	1.057147	CE_3^{Total}	1.359441

Table 4

(1) Estimated key parameters of the model; (2) estimated key parameters of the intracellular pathway.

(1)

Symbol	Value	Unit	Description
V_1	1.9608	nM/hr	Maximum activation velocity of Smad1/5 by BMP2 [1]
K_1	33.7255	nM	Michaelis activation coefficient of Smad1/5 by BMP2 [1]
d_1	1.0000	hr^{-1}	Decay rate of phosphorylated Smad1/5 [1]
V_2	40.0000	nM/hr	Maximum activation velocity of Smad2/3 by TGFβ [1]
K_2	10.0000	nM	Michaelis activation coefficient of Smad2/3 by TGFβ [9]
d_2	0.1961	hr^{-1}	Decay rate of phosphorylated Smad2/3 [9]
V_4	0.8198	nM/hr	Maximum activation velocity of Runx2 by Smad1/5 [9]
K_4	93.4510	nM	Michaelis activation coefficient of Runx2 by Smad1/5 [9]
V_5	0.8786	nM/hr	Maximum activation velocity of Runx2 by Smad2/3 [9]
K_5	9.8039	nM	Michaelis activation coefficient of Runx2 by Smad2/3 [9]
V_6	9.8039	nM/hr	Maximum activation velocity of Runx2 by β-catenin [9]
K_6	590.5882	nM	Michaelis activation coefficient of Runx2 by β-catenin [12]
d_1	36.8634	hr^{-1}	Degradation rate of Runx2 [12]
V_7	0.0519	nM/hr	Maximum activation velocity of Osx by Smad1/5 [12]
K_7	984.3137	nM	Michaelis activation coefficient of Osx by Smad1/5 [12]
V_8	0.0392	nM/hr	Maximum activation velocity of Osx by Runx2 [12]
K_8	139.2157	nM	Michaelis activation coefficient of Osx by Runx2 [12]
d_s	0.0224	hr^{-1}	Degradation rate of Osx [12]
S_p	450.0000	m/s	Speed of propagation of sound in immature bone [12]
S_a	720.0000	m/s	Speed of propagation of sound in mature bone [12]

(2)

Parameter	Mesenchymal stem cell		Pre-osteoblast		Active osteoblast	
	Spearman ρ	p value	Spearman ρ	p value	Spearman ρ	p value
V_6	0.6512	0.7985	0.5201	5.2047×10^{-3}	0.3719	1.5261×10^{-3}

(2)

Parameter	Mesenchymal stem cell		Pre-osteoblast		Active osteoblast	
	Spearman ρ	p value	Spearman ρ	p value	Spearman ρ	p value
V_2	0.1839	2.4592	0.1459	3.6012	−0.3596	6.1427
K_6	0.4116	0.8583	0.5206	2.3935×10^{-2}	0.1216	0.0003
K_2	−0.7195	3.0152	0.7633	4.9112	0.1769	3.5903
d_1	0.3552	0.7985	−0.0178	7.561×10^{-5}	0.3819	4.7219×10^{-5}
d_2	−0.1268	0.8916	0.3145	1.3927	0.1181	0.9265
V_8	0.9816	5.3071	0.9761	6.3275	0.8995	1.6231×10^{-6}
d_s	0.5545	2.7046	0.5103	1.091	0.6534	3.1659×10^{-4}
S_p	0.8912	0.0152	0.4169	3.5916×10^{-3}	0.6051	2.6719×10^{-3}
S_a	0.9609	0.0429	0.9872	5.6201×10^{-3}	0.9910	1.9602×10^{-3}

Table 5

(1) Orthogonal test data; (2) optimal combination analysis; (3) analysis of variance

(1)

Factor	Wnt dose A	BMP2 dose B	VEGF dose C	OBa number Without mechanical stimulation	OBa number With mechanical stimulation
1	0	0	0	1791	2397
2	0	5	5	13714	15156
3	0	10	10	13679	14815
4	5	0	5	2535	2918
5	5	5	10	14156	16156
6	5	10	0	13310	14167
7	10	0	10	2486	2769
8	10	5	0	13131	13982
9	10	10	5	13773	14107

(2)

K-value	Without mechanical stimulation			With mechanical stimulation		
K_1	29184	6812	28232	32368	8084	30546
K_2	30001	41001	30022	33241	45294	32181
K_3	28390	40762	30321	30858	43089	33740
k_1 = (K1/3)	9728	2270.6	9410.7	10789.3	2694.7	10182
k_2 = (K2/3)	10000.3	13667	10007.3	11080.3	15098	10727
k_3 = (K3/3)	9463.3	13596.3	10107	10286	14363	11246.7
Range	537	11396.4	2089	796.3	11403.3	1064.7
Optimal solution	A2	B2	C3	A2	B2	C3